ELSEVIER

Journal of Biomechanics 40 (2007) 2537–2542

JOURNAL OF BIOMECHANICS

www.elsevier.com/locate/jbiomech
www.JBiomech.com

A digital database of wrist bone anatomy and carpal kinematics

Douglas C. Moore, Joseph J. Crisco*, Theodore G. Trafton, Evan L. Leventhal

Bioengineering Laboratory, Department of Orthopaedics, Brown Medical School/Rhode Island Hospital, CORO West, Suite 404, 1 Hoppin Street, Providence, RI 02903, USA

Accepted 31 October 2006

Abstract

The skeletal wrist consists of eight small, intricately shaped carpal bones. The motion of these bones is complex, occurs in three dimensions, and remains incompletely defined. Our previous efforts have been focused on determining the in vivo three-dimensional (3-D) kinematics of the normal and abnormal carpus. In so doing we have developed an extensive database of carpal bone anatomy and kinematics from a large number of healthy subjects. The purpose of this paper is to describe that database and to make it available to other researchers. CT volume images of both wrists from 30 healthy volunteers (15 males and 15 females) were acquired in multiple wrist positions throughout the normal range of wrist motion. The outer cortical surfaces of the carpal bones, radius and ulna, and proximal metacarpals were segmented and the 3-D motion of each bone was calculated for each wrist position. The database was constructed to include high-resolution surface models, measures of bone volume and shape, and the 3-D kinematics of each segmented bone. The database does not include soft tissues of the wrist. While there are numerous digital anatomical databases, this one is unique in that it includes a large number of subjects and it contains in vivo kinematic data as well as the bony anatomy.

Keywords: Database; Digital; Wrist; Bone; Position

1. Introduction

With the establishment of the Visible Human Project in 1989, the National Library of Medicine ushered in the era of digital anatomy and the use of electronic images for medical education, clinical medicine and biomedical research (Bitsakos et al., 2005; Garner and Pandy, 1999, 2001; Teran et al., 2005). In 1994, the Visible Human Male dataset was released, followed by the Visible Human Female in 1995. Both included axial CT, axial (head and neck) and longitudinal MRI, and high-resolution color photographs of serial axial cross-sections of a single individual in one position. The current challenge is to include information on function with the three-dimensional (3-D) structural information, and to add data to represent normal phenotypic variability.

The primary function of the musculoskeletal system is to facilitate motion. At present there are few datasets that include accurate models of bony anatomy registered to patient-specific in vivo kinematic data. With recent advances in imaging and image analysis, however, this has begun to change. Several investigators have begun to link accurate CT-generated bone models directly to bone-specific in vivo kinematic data (Crisco et al., 1999; Feipel et al., 1992; Tashman and Anderst, 2003). For example, Tashman et al. have developed a system for measuring joint motion in vivo using CT-generated bone models and high frame-rate stereo videography (Tashman and Anderst, 2003). They have used the technique to evaluate knee motion after anterior cruciate ligament reconstruction (Tashman et al., 2004), and to estimate articular cartilage behavior during dynamic loading from proximity maps of the subchondral bone (Anderst and Tashman, 2003). Other investigators have used serial CT scanning and markerless registration techniques to analyze carpal (Crisco et al., 2005a; Feipel and Rooze, 1999; Moojen et al., 2002) and forearm bone motion (Moore et al., 2002) as the hand is positioned in 3-D space. Markerless carpal bone registration has also been performed using serial images acquired via magnetic resonance imaging (Moritomo et al., 2004).

*Corresponding author. Tel.: +1 401 444 4231; fax: +1 401 444 4418.
E-mail address: joseph_crisco@brown.edu (J.J. Crisco).

0021-9290/$ - see front matter © 2006 Published by Elsevier Ltd.
doi:10.1016/j.jbiomech.2006.10.041

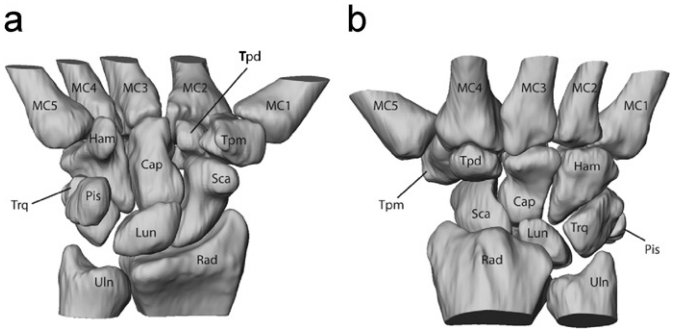

Fig. 1. Volar (a) and dorsal (b) views of the bones from a right wrist. The eight carpal bones, radius, ulna, and five metacarpals are rendered using triangular mesh models of the outer cortical bone surface segmented from a CT volume image. The abbreviations for each bone are described in the text.

The efficient sharing of musculoskeletal kinematic data has the potential to hasten advances in musculoskeletal biomechanics. Only by sharing data will it be possible to assemble datasets that include kinematic and model information from large numbers of volunteers. Large datasets are necessary to accurately reflect normal anatomic and kinematic variability. But the real potential of data sharing is that it facilitates collaboration and it *enables* "distributed analysis," both of which have tremendous leveraging potential. While the benefit of collaboration is obvious, with distributed analysis a single large dataset can be analyzed by multiple investigators (or groups) with different goals and interests, who may or may not have a formal collaborative agreement. For example, data generated by one group interested in bony kinematics could be used by a second group interested in solid mechanics (e.g. finite element analysis, or FEA), or a third group interested in soft tissue modeling.

In this paper, we describe the creation of a digital anatomic and kinematic database focused on the eight carpal bones of the wrist (Fig. 1) consisting of data from both wrists of 30 healthy volunteers in various isolated and combined positions of wrist flexion, extension, and radial and ulnar deviation. The database contains patient-specific measures of bone shape, bone surface models and 3-D kinematic data.

2. Methods

2.1. Subjects

With human subjects approval, study volunteers were recruited and informed consent was obtained. The subjects were recruited as controls for two different studies with slightly different scanning protocols (described below). Volunteers were pre-screened for a history of wrist trauma after which they were examined by a board certified orthopedic hand surgeon, including active range of motion, grip strength, and bilateral posteroanterior and lateral plane radiographs. Only individuals with a history of wrist trauma, or signs of wrist pathology or obvious degenerative changes were excluded. Data from 30 subjects were included in the database, 15 females (ages 21–28) and 15 males (ages 22–34).

2.2. Scanning

Both wrists of each volunteer were imaged simultaneously with a GE helical CT scanner (GE Medical, Milwaukee, WI). During scanning, the volunteers were seated semi-prone behind the CT gantry with their extended forearms parallel to the long axis of the moving table. A custom-designed dual-protractor wrist-positioning jig was used to facilitate gross positioning of the wrists.

Different wrist positioning protocols were used for the original two studies, an "incremental orthogonal" protocol and a "combined motion" protocol. The incremental orthogonal protocol (5 males, 5 females) included scans at eight targeted positions, one with the wrist in neutral (dorsum of the third metacarpal aligned with the dorsal surface of the forearm), followed by subsequent scans with the wrist in 30° and 60° of flexion, 30° and 60° of extension, 20° and 40° of ulnar deviation, and 20° of radial deviation. The combined motion protocol (10 males, 10 females) included scans at nine targeted wrist positions, the first with the wrist in neutral, followed by scans at 40° of flexion, 40° of extension, 10° of radial deviation, 30° of ulnar deviation, and combined motions of 40° flexion and 30° ulnar deviation, 40° extension and 30° ulnar deviation, 40° extension and 10° radial deviation, and 40° flexion and 10° radial deviation.

Contiguous 1.0 mm slice images were acquired of the distal forearm, wrist, and proximal metacarpus, including 1–2 cm of the distal radius and ulna, the entire carpus, and 1–2 cm of the proximal portion of the metacarpals (typically 60–80 individual slice images). Scanning was performed at 80–120 kVp and 80 mAs, with a 48 cm field of view, yielding individual slice images with an isometric pixel resolution of $0.9 \times 0.9\,\text{mm}^2$. The neutral scans were reconstructed using a 12–16 cm field of view, yielding one set of high-resolution images for each subject, with pixel resolutions ranging from 0.2×0.2 to $0.3 \times 0.3\,\text{mm}^2$.

2.3. Bone segmentation and surface reconstruction

Digital models of the bone surfaces were generated from the high-resolution neutral position CT reconstructions of each wrist using a combination of commercially available and custom-written software (Fig. 2). A slice-by-slice set of points representing the bone surface topography was generated using the thresholding and edge detection algorithms in Analyze™ (Mayo Clinic Foundation, Rochester, MN) image processing software (Fig. 2A). The contours were then stacked,

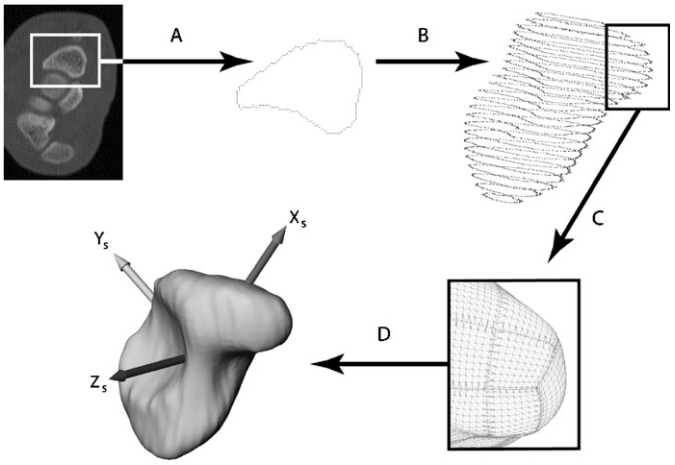

Fig. 2. The bones of the wrist are segmented from CT volumes images by first identifying the 2-D outer cortical bone contours in each image slice (A). The contours are identified and collected into a single 3-D point cloud for each bone (B). From these 3-D points a triangular mesh is constructed (C). Bone volume and inertial properties are then computed from the triangular mesh model of this typical scaphoid bone (D). The three principal axes (X_S, Y_S, and Z_S) are shown here, emanating from the bone's centroid.

edited and grouped using custom software routines written in MatLab (Mathworks, Natick, MA) and C++, yielding separate 3-D point cloud for each bone (Fig. 2B). The left wrists were "converted" to right wrists to simplify the kinematic analysis. This was done by inverting the X component of the bone surface coordinates and reversing the direction of the surface contours in each image slice. Surfaces were then generated for each bone by tiling the point clouds with triangles, followed by manual editing, smoothing and fitting with a mosaic of individual NURBS patches (Fig. 2C) using Geomagic software (Raindrop Geomagic, Research Triangle Park, NC). The bone surfaces were saved in ASCII files in the Open Inventor format, which includes the 3-D coordinates of each vertex point and the connectivity of the triangular patches. The x, y and z coordinates of each vertex, and the variables calculated from these surface models, are reported in a with respect to the CT scanner's built-in global coordinate system, which sets the z-axis parallel to the CT table and the x- and y-axes horizontal and vertical, respectively.

The volume (mm^3), centroid location (mm), and the magnitude and orientation of the principal inertial axes (normalized unit vectors) for each bone were calculated from the smoothed, neutral-position surface models (Fig. 2D) using MatLab code based on Gauss's divergence theorem (Eberly et al., 1991; Gonzalez-Ochoa et al., 1998; Messner and Taylor, 1980); the inertia magnitudes were calculated as if the bones were uniformly dense solids (with density arbitrarily set to a unit value of 1). As with the bone surfaces, the bone volume centroids and principal inertial axes are reported in terms of the CT scanner's global coordinate system. Ordering of the inertia magnitudes and the sense of each inertial axis was defined using a standardized method based on a radius-based anatomic coordinate system (Coburn et al., 2006). Note, however, that the volumes, centroid locations and inertial axes for the radius, ulna and five metacarpals do not reflect whole bone properties since these long bones were incompletely imaged during CT scanning.

2.4. Kinematic transforms

The positions of the bones at each non-neutral wrist position were calculated with respect to the neutral wrist position, assuming rigid body kinematics

$$B_i = R_i \times B_0 + T_i, \quad (1)$$

where B_0 is the bone in the neutral position and B_i is the bone in wrist position i, R_i is the 3×3 rotation matrix and T_i is the 1×3 translation vector. Two different methods were used to generate the kinematic transforms: the first required segmentation of every bone at every wrist position and used inertia matching and closest point algorithms (Crisco and McGovern, 1998; Crisco et al., 1999) while our more recent approach has involved the use of a semi-automated algorithm that employs tissue-classified distance fields for calculating the bone kinematics (Marai et al., 2006). As with the bone surface and centroid data, the position and kinematic data are reported in terms of the CT scanner's global coordinate system.

2.5. Database file structure and contents

The database is organized by subject, with data from each subject contained in a separate folder labeled with a randomly generated five digit number (e.g. 12345) to satisfy HIPAA confidentiality requirements. The dataset for each subject includes brief demographic descriptors (age and gender); data for wrist range of motion and grip strength; surface models, volumes, centroid coordinates, inertia magnitudes and inertial principal axes for each bone; and a series of kinematic transforms that locate each of the bones with respect to their neutral positions for each subsequent wrist position. All of the data is provided in ASCII format, with file names, format and folder structure described in detail on the supplementary website (supplementary data associated with this article can be found in the online version at doi:10.1016/j.jbiomech.2006.10.041). In all cases where bone-specific data is listed sequentially (i.e. volume, inertial or kinematic data), it is presented in the following order: radius, ulna, scaphoid, lunate, triquetrum, pisiform, trapezoid, trapezium, capitate, hamate, metacarpal 1, metacarpal 2, metacarpal 3, metacarpal 4, and metacarpal 5.

For additional data and periodic updates, contact the authors directly.

3. Results

Both wrists of 30 healthy volunteers were scanned, yielding 520 volume images for analysis; 60 neutral position images and 460 images with the wrists in various positions of flexion, extension, and radial and ulnar deviation. Sixty sets for each of the 15 bones in the wrist were segmented. A total of 894 bone surface models were successfully generated from the neutral position scans (six individual bones—three metacarpals, two ulnae, and one trapezoid—from the entire dataset were incompletely scanned and therefore surface models were not constructed for these). There were 894 values of bone volume, centroid and principal inertial data; values for the incompletely scanned radii, ulnae and metacarpals are not valid. Our kinematic analysis yielded 460 transforms that describe the position of each bone with respect to the same bone in the neutral wrist position.

Despite targeting only 16 wrist positions, analysis of our data revealed that we actually scanned wrist positions distributed throughout the full range of wrist motion, from 70° extension to 40° ulnar deviation to 60° of flexion, and 30° of radial deviation (Fig. 3). This distribution of positions resulted from the error associated with using a protractor device to define wrist position. Therefore, when wrist position is defined anatomically as the orientation of the capitate with respect to the radius (Crisco et al., 2005a), the 16 targeted wrist positions actually yielded 520 different wrist positions.

Our data includes a continuum of wrist and carpal bone sizes. As one would expect, the carpal bones of the female volunteers were smaller on average than those of the males (by an average of 33.3%), but the carpal volumes of the largest females were similar to the carpal volumes of the smallest males. Interestingly, we have found that the dimensions of the individual carpal bones of men and women are comparably sized (when normalized by carpal volume) and that they tend to scale isometrically (Crisco et al., 2005b). This suggests that there are no large, systematic, gender-specific differences in bone size between men and women, though it does not rule out the existence of smaller local differences in shape or curvature.

4. Discussion

In this paper, we describe the creation of a digital database of wrist bone anatomy and in vivo carpal kinematics from both wrists of 30 healthy volunteers, which encompasses the full wrist range of motion. To our knowledge, this is the first publicly available database that contains both accurate digital anatomic models of bony

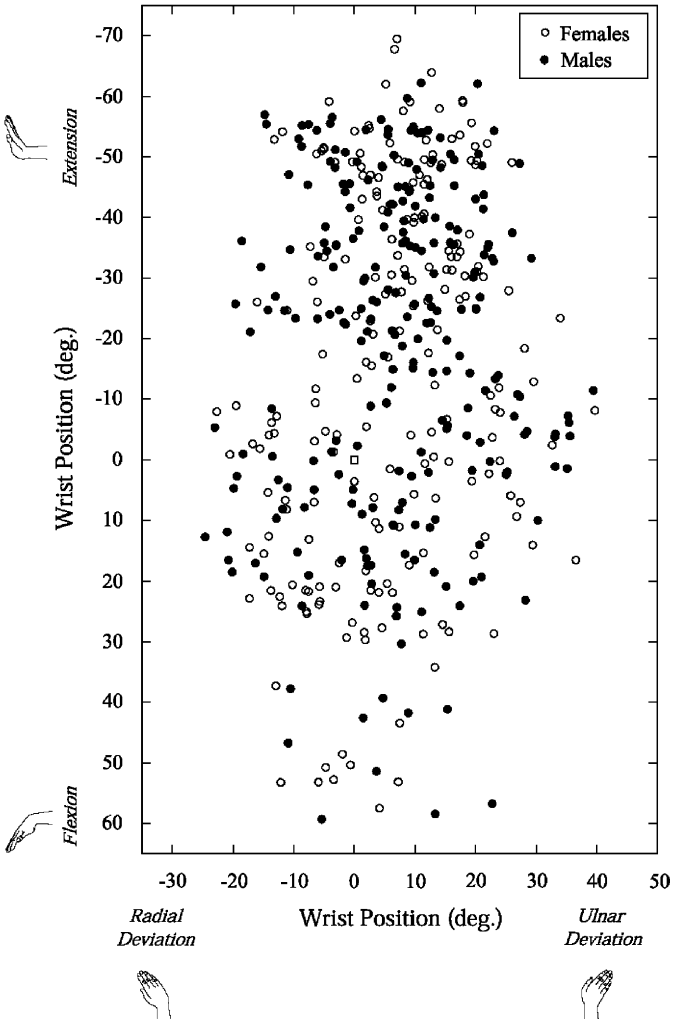

Fig. 3. The wrist positions, as defined by the orientation of the capitate, of both wrists for all subjects included in the database.

anatomy and matched, subject-specific in vivo kinematic data. Our goal is to make this information widely available, for use in research and education, as well as for commercial applications aimed at improving health care.

Our purpose in sharing the data is to foster collaboration and encourage analysis by other interested investigators. To this point our analysis of wrist kinematics has largely been focused on the kinematics of the radiocarpal joint, though we have also looked at scaphotrapezio–trapezoidal kinematics in some detail (Sonenblum et al., 2004). There are numerous other articulations in the carpus that to date have received only limited study, with few reports in the literature. Similarly, our analysis of carpal bone shape has focused on the relatively simple metrics of overall size (bounding box dimensions) and scaling, when clearly there is an immense amount of unexplored shape and curvature information captured in the dataset. Finally, we have not yet used the data for any wrist model development or structural analysis. Our dataset provides a large library of bone shapes and postures that make it useful for kinematic or structural (finite element) modeling, given appropriate assumptions and model construction.

The two primary strengths of the database are its comprehensiveness and the direct linking of anatomy to subject specific kinematic data. The database contains data on 60 healthy wrists (30 subjects) from 15 females and 15 males, ranging in age from 21 to 34, including 894 bone surface models and 520 separate wrist positions. This is by far the largest database of carpal (or other) anatomy available to date. Further, it is currently the only publicly available database that links data on musculoskeletal function (kinematics) to subject-specific anatomic data. This feature is a powerful next step in the evolution of musculoskeletal functional analysis.

Beyond the size and comprehensiveness of the dataset, an additional strength is its accuracy (Crisco and McGovern, 1998; Marai et al., 2006; Neu et al., 2000). Briefly, when the same carpal bones were repeatedly segmented from multiple distinct volume images, the larger carpal bones (mean volume approx. 2966 mm^3) had 0.8% standard deviation in volume calculation, while the smaller bones (mean volume 669 mm^3) had a 4.8% standard deviation in volume calculation (Neu et al., 2000). In this same error analysis the variation in the orientation of the second and third inertial axes was less than 1.5%. As with the other variables, kinematic accuracy was dependent upon the specific bone; rotation errors of the capitate and scaphoid were less than 0.5°, while those for the other bones were generally less than 2°. Translation errors were less than 1 mm (Neu et al., 2000). Our newer tissue classification approach to calculating rigid body kinematics is even more accurate (Marai et al., 2006).

Visualization of the bones at different wrist positions is crucial for the detailed analysis of carpal kinematics. Motion of the carpal bones is complex, even during relatively uncomplicated wrist motions. For example, Fig. 4 depicts the complex coupled motion of the capitate and scaphoid bones as wrist is moved from neutral to ulnar deviation. As expected, the capitate rotates ulnarly in the frontal plane, but the scaphoid rotates largely into extension. To characterize this motion, we calculate helical axes of rotation and describe the location of these rotation axes with respect to a radius-based coordinate system (X_R, Y_R, and Z_R). Capitate motion can be analyzed by studying the location and orientation of its rotation axis (A_C), which for ulnar deviation is parallel to the Z_R axis. The coupled extension motion of the scaphoid during ulnar deviation is apparent as its rotation axis (A_S) is parallel to the Y_R axis.

The continuousness of our dataset was somewhat serendipitous. Our initial goal was to collect and analyze kinematic data at discrete positions of wrist motion. This is why we developed our dual protractor wrist positioning system and implemented our discrete positioning protocol. However, we ultimately found $\pm 10°$ of error between the protractor predicted position and actual wrist position, as defined by the orientation of the third metacarpal or

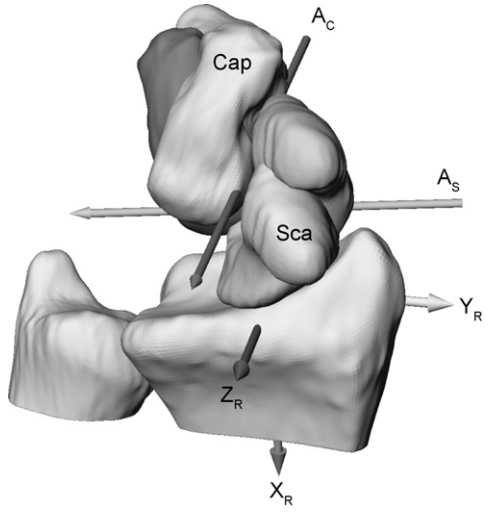

Fig. 4. Visualization of the complex, coupled motion of the capitate and scaphoid bones as the wrist is moved from neutral (labeled bones) to ulnar deviation (unlabeled bones). Here the scaphoid rotates into extension as the capitate (and the wrist) rotates ulnarly in the frontal plane. The capitate (A_C) and scaphoid (A_S) rotation axes for this motion are also depicted, as are the axes of the radial coordinate system.

capitate (we have found that capitate and third metacarpal motion is nearly identical in that they track within $0.7^\circ \pm 4.4^\circ$ of one another (Neu et al., 2001)). Accordingly, for analytical purposes we use capitate position (calculated from our CT images) as our independent variable. While at first this seemed like a disadvantage, the result is a large, continuous dataset, which comprehensively covers the full range of wrist motion lending itself well to regression analysis. Our current approach for analyzing carpal kinematics involves the analysis of all subjects across the entire range of wrist motion (Crisco et al., 2005a). Using this methodology we have found very consistent—albeit complex—patterns of carpal kinematics in these healthy individuals. However, subtle nonlinear relationships between wrist and carpal motion are not be captured with this database.

Our selection of CT imaging to generate our bone models was based on considerations of accuracy and availability. However, the use of CT has several disadvantages. First, because CT imaging is relatively slow we were limited to generating data from CT images at static wrist postures. Our assumption is that our static data approximates dynamic carpal motion. We think this is reasonable given that the carpus is essentially passive and other investigators have found only minimal (0°–2.5°) hysteresis during dynamic wrist motion (Short et al., 1997). Also, because CT uses ionizing radiation, the number of imagable positions is limited for each individual. So, while we have a large number of total positions in the database, for each subject there is data on at most 10 positions.

In summary, we have described a comprehensive digital anatomic database of the normal healthy carpus that includes information on bony anatomy and kinematics. Despite its limitations, it is the first and largest database of its kind, incorporating data on normal phenotypic variability as well as function. Use of this data by other investigators and educators has the potential to hasten the advances in our understanding of complex wrist biomechanics.

Acknowledgment

This study was supported by NIH AR44005.

References

Anderst, W.J., Tashman, S., 2003. A method to estimate in vivo dynamic articular surface interaction. Journal of Biomechanics 36 (9), 1291–1299.

Bitsakos, C., Kerner, J., Fisher, I., Amis, A.A., 2005. The effect of muscle loading on the simulation of bone remodelling in the proximal femur. Journal of Biomechanics 38 (1), 133–139.

Coburn, J.C., Upal, M.A., Crisco, J.J., 2006. Coordinate systems for the carpal bones of the wrist. Journal of Biomechanics.

Crisco, J.J., McGovern, R.D., 1998. Efficient calculation of mass moments of inertia for segmented homogenous three-dimensional objects. Journal of Biomechanics 31, 97–101.

Crisco, J.J., McGovern, R.D., Wolfe, S.W., 1999. Noninvasive technique for measuring in vivo three-dimensional carpal bone kinematics. Journal of Orthopedic Research 17 (1), 96–100.

Crisco, J.J., Coburn, J.C., Moore, D.C., Akelman, E., Weiss, A.P., Wolfe, S.W., 2005a. In vivo radiocarpal kinematics and the Dart Thrower's motion. Journal of Bone and Joint Surgery—American Volume 87 (12), 2729–2740.

Crisco, J.J., Coburn, J.C., Moore, D.C., Upal, M.A., 2005b. Carpal bone size and scaling in men versus in women. Journal of Hand Surgery—American Volume 30 (1), 35–42.

Eberly, D., Lancaster, J., Alyassin, A., 1991. On gray scale image measurements: II. Surface area and volume. CVGIP: Graphical Models and Image Processing 53 (6), 550–562.

Feipel, V., Rooze, M., 1999. Three-dimensional motion patterns of the carpal bones: an in vivo study using three-dimensional computed tomography and clinical applications. Surgical and Radiological Anatomy 21 (2), 125–131.

Feipel, V., Rooze, M., Louryan, S., Lemort, M., 1992. Bi- and three-dimensional CT study of carpal bone motion occurring in lateral deviation. Surgical and Radiological Anatomy 14, 341–348.

Garner, B.A., Pandy, M.G., 1999. A kinematic model of the upper limb based on the visible human project (VHP) image dataset. Computer Methods in Biomechanics and Biomedical Engineering 2 (2), 107–124.

Garner, B.A., Pandy, M.G., 2001. Musculoskeletal model of the upper limb based on the visible human male dataset. Computer Methods in Biomechanics and Biomedical Engineering 4 (2), 93–126.

Gonzalez-Ochoa, C., McCammon, S., Peters, J., 1998. Computing moments of objects enclosed by piecewise polynomial surfaces. ACM Transactions on Graphics (TOG) 17 (3), 143–157.

Marai, G.E., Laidlaw, D.H., Crisco, J.J., 2006. Super-resolution registration using tissue-classified distance fields. IEEE Transactions on Medical Imaging 25 (2), 1–11.

Messner, A.M., Taylor, G.Q., 1980. Algorithm 550: solid polyhedron measures [Z]. ACM Transactions on Mathematical Software (TOMS) 6 (1), 121–130.

Moojen, T.M., Snel, J.G., Ritt, M.J., Kauer, J.M., Venema, H.W., Bos, K.E., 2002. Three-dimensional carpal kinematics in vivo. Clinical Biomechanics (Bristol, Avon) 17 (7), 506–514.

Moore, D.C., Hogan, K.A., Crisco 3rd, J.J., Akelman, E., Dasilva, M.F., Weiss, A.P., 2002. Three-dimensional in vivo kinematics of the distal radioulnar joint in malunited distal radius fractures. Journal of Hand Surgery—American Volume 27 (2), 233–242.

Moritomo, H., Murase, T., Goto, A., Oka, K., Sugamoto, K., Yoshikawa, H., 2004. Capitate-based kinematics of the midcarpal joint during wrist radioulnar deviation: an in vivo three-dimensional motion analysis. Journal of Hand Surgery—American Volume 29 (4), 668–675.

Neu, C.P., McGovern, R.D., Crisco, J.J., 2000. Kinematic accuracy of three surface registration methods in a three-dimensional wrist bone study. Journal of Biomechanical Engineering 122 (5), 528–533.

Neu, C.P., Crisco, J.J., Wolfe, S.W., 2001. In vivo kinematic behavior of the radio–capitate joint during wrist flexion-extension and radio–ulnar deviation. Journal of Biomechanics 34 (11), 1429–1438.

Short, W.H., Werner, F.W., Fortino, M.D., Mann, K.A., 1997. Analysis of the kinematics of the scaphoid and lunate in the intact wrist joint. Hand Clinics 13 (1), 93–108.

Sonenblum, S.E., Crisco, J.J., Kang, L., Akelman, E., 2004. In vivo motion of the scaphotrapezio–trapezoidal (STT) joint. Journal of Biomechanics 37 (5), 645–652.

Tashman, S., Anderst, W., 2003. In-vivo measurement of dynamic joint motion using high speed biplane radiography and CT: application to canine ACL deficiency. Journal of Biomechanical Engineering 125 (2), 238–245.

Tashman, S., Collon, D., Anderson, K., Kolowich, P., Anderst, W., 2004. Abnormal rotational knee motion during running after anterior cruciate ligament reconstruction. American Journal of Sports Medicine 32 (4), 975–983.

Teran, J., Sifakis, E., Blemker, S.S., Ng-Thow-Hing, V., Lau, C., Fedkiw, R., 2005. Creating and simulating skeletal muscle from the visible human data set. IEEE Transactions on Visualization and Computer Graphics 11 (3), 317–328.